

# Reservoir Subspace Injection for Online ICA under Top- $n$ Whitening

Wenjun Xiao, Yuda Bi, Vince Calhoun, *Fellow, IEEE*

**Abstract**—Reservoir expansion can improve online independent component analysis (ICA) under nonlinear mixing, yet top- $n$  whitening may discard injected features. We formalize this bottleneck as *reservoir subspace injection (RSI)*: injected features help only if they enter the retained eigenspace without displacing passthrough directions. RSI diagnostics (IER, SSO,  $\rho_x$ ) identify a failure mode in our top- $n$  setting: stronger injection increases IER but crowds out passthrough energy ( $\rho_x: 1.00 \rightarrow 0.77$ ), degrading SI-SDR by up to 2.2 dB. A guarded RSI controller preserves passthrough retention and recovers mean performance to within 0.1 dB of baseline  $1/N$  scaling. With passthrough preserved, RE-OICA improves over vanilla online ICA by +1.7 dB under nonlinear mixing and achieves positive SI-SDR<sub>sc</sub> on the tested super-Gaussian benchmark (+0.6 dB).

**Index Terms**—Blind source separation, independent component analysis, reservoir computing, echo state network, online learning, natural gradient

## I. INTRODUCTION

Independent component analysis (ICA) recovers latent independent sources from their linear mixtures and, under the standard linear instantaneous mixing model, is identifiable whenever at most one source is Gaussian [1], [2]. Classical batch algorithms—Infomax [3], FastICA [4], JADE [5]—have been deployed extensively in neuroimaging [6], [7], telecommunications, and audio processing; see [8], [9] for surveys and textbook treatment [2]. However, batch ICA requires full data and a fixed mixing matrix, motivating sample-wise online ICA. Amari’s natural gradient [10], [11] provides an equivariant update with reduced sensitivity to mixing conditioning, and online recursive ICA (ORICA) combines recursive-least-squares whitening with natural-gradient updates for real-time EEG source separation [12]. Our vanilla online ICA is ORICA-inspired, not a full reimplementation: it keeps ORICA’s natural-gradient demixing update [12] but replaces RLS whitening with EMA covariance and periodic eigendecomposition (every 64 steps). It is the reservoir-free RE-OICA ablation and is intended to isolate RSI effects rather than provide a head-to-head ORICA benchmark. Stochastic-approximation methods further extend online ICA to tensorial

or multivariate-component settings [13], [14], [15]. Nevertheless, these approaches operate in the observation space: under nonlinear mixing or nonlinear source distortions [16], [17], a purely *linear* demixing in  $\mathbf{x}$  can be insufficient. Nonlinear ICA typically requires auxiliary variables or temporal structure for identifiability [18], [19], [20], while deep-learning solutions often sacrifice online, low-latency processing.

Reservoir computing [21], [22] offers an alternative to observation-space demixing: an echo-state network (ESN) maps inputs into fixed high-dimensional nonlinear features, approximating fading-memory functionals [23]. Recent results relate ESNs to kernel and random-feature views of nonlinear dynamics [24], [25]. Reservoir-based separation has been explored for offline denoising with a trained readout [26]; in contrast, reservoir-expanded online ICA (RE-OICA) targets fully online, sample-by-sample blind source separation (BSS) with no reservoir/readout training. A practical issue is that low-latency online pipelines typically apply top- $n$  whitening, which can discard injected reservoir features; without retention diagnostics, it is difficult to determine when expansion is beneficial.

This gap motivates the present work. We recast reservoir-expanded online ICA as a *subspace-injection* problem and contribute:

- (i) RSI diagnostics (IER, SSO,  $\rho_x$ ) that quantify injected-feature retention and passthrough preservation under top- $n$  whitening.
- (ii) A crowd-out mechanism—validated in controlled experiments (10 seeds, SI-SDR<sub>sc</sub>)—showing that stronger injection can raise IER yet reduce  $\rho_x$  and degrade SI-SDR; improvements under nonlinear mixing occur when passthrough is preserved.
- (iii) A crowd-out-guarded controller that adapts  $\alpha_t$  to maintain high  $\rho_x$  while allowing beneficial injection, with negligible overhead beyond whitening eigendecomposition.

## II. MODEL AND MAIN RESULTS

### A. Setup and Notation

We observe  $\mathbf{x}_t \in \mathbb{R}^n$  generated from  $n$  independent sources  $\mathbf{s}_t \in \mathbb{R}^n$  with  $\mathbb{E}[\mathbf{s}_t] = \mathbf{0}$ ,  $\mathbb{E}[\mathbf{s}_t \mathbf{s}_t^\top] = \mathbf{I}_n$ , and finite fourth moments. We consider:

$$\text{(Static) } \mathbf{x}_t = \mathbf{A} \mathbf{s}_t, \quad (1)$$

$$\text{(Time-varying) } \mathbf{x}_t = \mathbf{A}(t) \mathbf{s}_t, \quad \mathbf{A}(t) = \mathbf{A}_0 + \varepsilon \sin\left(\frac{2\pi ft}{T}\right) \Delta, \quad (2)$$

$$\text{(Nonlinear) } \mathbf{x}_t = g(\mathbf{A} \mathbf{s}_t) + \eta_t, \quad (3)$$

W. Xiao is with the Department of Computer Science, The George Washington University, Washington, DC 20052 USA.

Y. Bi is with the Tri-Institutional Center for Translational Research in Neuroimaging and Data Science (TReNDS), Georgia State University, Georgia Institute of Technology, and Emory University, Atlanta, GA 30303 USA (e-mail: ybi@gsu.edu).

V. D. Calhoun is with the Tri-Institutional Center for Translational Research in Neuroimaging and Data Science (TReNDS), Georgia State University, Georgia Institute of Technology, and Emory University, Atlanta, GA 30303 USA, and also with the School of Electrical and Computer Engineering, Georgia Institute of Technology, Atlanta, GA 30332 USA (e-mail: vcalhoun@gsu.edu).

where  $\mathbf{A}, \mathbf{A}_0, \Delta \in \mathbb{R}^{n \times n}$ ,  $g$  is component-wise Lipschitz (e.g., tanh),  $\eta_t$  is i.i.d. Gaussian,  $f$  is the modulation frequency, and  $T$  is the sequence horizon used for normalization.

RE-OICA uses a fixed reservoir and projection, concatenates passthrough and injected features, then applies top- $n$  whitening and natural-gradient ICA:

$$\begin{aligned} \mathbf{r}_t &= \text{ESN}(\mathbf{x}_{1:t}) \in \mathbb{R}^N, \\ \mathbf{p}_t &= c_N \mathbf{W}_{\text{read}} \mathbf{r}_t \in \mathbb{R}^d, \quad \mathbf{u}_t = [\mathbf{x}_t; \alpha_t \mathbf{p}_t] \in \mathbb{R}^{n+d}, \\ \mathbf{z}_t &= \text{Whiten}_n(\mathbf{u}_t) \in \mathbb{R}^n, \quad \mathbf{y}_t = \text{ICA}(\mathbf{z}_t) \in \mathbb{R}^n, \end{aligned} \quad (4)$$

where  $\alpha_t$  is the RSI-controlled injection scale (defined below). Unless stated otherwise,  $n=3$ ,  $N=500$ ,  $d=20$ . We use top- $k$  whitening with  $k=n$  throughout.

### B. Reservoir Encoding

We use a sparse echo-state network (ESN) reservoir [21], [27], [28] with fixed random weights. Let  $\mathbf{W}_{\text{in}} \in \mathbb{R}^{N \times n}$ ,  $\mathbf{W}_{\text{res}} \in \mathbb{R}^{N \times N}$  (sparse, spectral radius  $\rho$ ), and  $\mathbf{b} \in \mathbb{R}^N$ . The state update is

$$\mathbf{r}_t = (1 - \alpha_r) \mathbf{r}_{t-1} + \alpha_r \sigma(\mathbf{W}_{\text{in}} \mathbf{x}_t + \mathbf{W}_{\text{res}} \mathbf{r}_{t-1} + \mathbf{b}), \quad (5)$$

with leak rate  $\alpha_r \in (0, 1]$  and  $\sigma = \tanh$  applied element-wise.

**Proposition 1** (Echo State Property). *Let  $\sigma$  be  $L_\sigma$ -Lipschitz. If  $\rho_{\text{eff}} := (1 - \alpha_r) + \alpha_r L_\sigma \|\mathbf{W}_{\text{res}}\| < 1$ , then for any two initial states  $\mathbf{r}_0, \mathbf{r}'_0$  driven by the same input,  $\|\mathbf{r}_t - \mathbf{r}'_t\| \leq \rho_{\text{eff}}^t \|\mathbf{r}_0 - \mathbf{r}'_0\|$ .*

*Proof.* Let  $\mathbf{a}_t = \mathbf{W}_{\text{in}} \mathbf{x}_t + \mathbf{b}$ . By Lipschitzness,

$$\begin{aligned} \|\mathbf{r}_t - \mathbf{r}'_t\| &\leq (1 - \alpha_r) \|\mathbf{r}_{t-1} - \mathbf{r}'_{t-1}\| + \alpha_r L_\sigma \|\mathbf{W}_{\text{res}}\| \|\mathbf{r}_{t-1} - \mathbf{r}'_{t-1}\| \\ &= \rho_{\text{eff}} \|\mathbf{r}_{t-1} - \mathbf{r}'_{t-1}\|. \end{aligned}$$

Iterating yields the claim.  $\square$

Using the induced operator norm in  $\|\mathbf{W}_{\text{res}}\|$  gives a sufficient (possibly conservative) contraction condition. Thus the dependence on the initial state decays exponentially (fading memory).

**Readout projection and passthrough.** With fixed random  $\mathbf{W}_{\text{read}} \in \mathbb{R}^{d \times N}$ , define  $\mathbf{p}_t = c_N \mathbf{W}_{\text{read}} \mathbf{r}_t \in \mathbb{R}^d$  and  $\mathbf{u}_t = [\mathbf{x}_t; \alpha_t \mathbf{p}_t] \in \mathbb{R}^{n+d}$ . This reduces whitening cost from  $O(N^3)$  to  $O((n+d)^3)$  while preserving a raw-input floor. We test  $c_N \in \{1/N, 1/\sqrt{N}\}$ ; effective injection magnitude is  $\alpha_t c_N$ , with  $c_N$  fixed per branch and  $\alpha_t$  adapted only at whitening refreshes.

### C. Motivation: Random-Feature Approximation

Random-feature expansion [29], [30] motivates reservoir lifting in nonlinear demixing, but the operational bottleneck here is retention after top- $n$  whitening.

**Proposition 2** (Motivational linearization bound). *Under standard random-feature integral-representation assumptions for  $\psi = \mathbf{A}^{-1} \circ g^{-1}$ , the population-optimal linear readout from  $N$  memoryless random features obeys, where  $\Phi: \mathbb{R}^n \rightarrow \mathbb{R}^N$  is the random-feature map and  $B$  bounds the integral-representation coefficient norm:*

$$\mathbb{E}_{\mathbf{W}_{\text{in}}, \mathbf{b}} \left[ \min_{\mathbf{M}} \mathbb{E}_{\mathbf{x}} \left[ \|\mathbf{M} \Phi(\mathbf{x}) - \mathbf{s}\|^2 \right] \right] \leq \frac{nB^2}{N}. \quad (6)$$

*Remark.* Proposition 2 is an in-principle population result for memoryless features. Our core contribution is top- $n$  retention diagnostics and control in the online recurrent pipeline.

### D. Reservoir Subspace Injection (RSI)

We form the whitening input

$$\mathbf{u}_t = [\mathbf{x}_t; \alpha_t \mathbf{p}_t], \quad \mathbf{p}_t = c_N \mathbf{W}_{\text{read}} \mathbf{r}_t, \quad (7)$$

and let  $\mathbf{V}_n \in \mathbb{R}^{(n+d) \times n}$  be the top- $n$  eigenvectors of  $\mathbf{C}_t(\alpha_t)$  at each whitening refresh. Define the unscaled concatenation  $\tilde{\mathbf{u}}_t = [\mathbf{x}_t; \mathbf{p}_t]$  with block covariance

$$\tilde{\mathbf{C}}_t = \text{Cov}(\tilde{\mathbf{u}}_t) = \begin{bmatrix} \mathbf{C}_{xx} & \mathbf{C}_{xp} \\ \mathbf{C}_{px} & \mathbf{C}_{pp} \end{bmatrix}.$$

Under injection,  $\mathbf{u}_t = [\mathbf{x}_t; \alpha_t \mathbf{p}_t]$  has covariance

$$\mathbf{C}_t(\alpha_t) = \begin{bmatrix} \mathbf{C}_{xx} & \alpha_t \mathbf{C}_{xp} \\ \alpha_t \mathbf{C}_{px} & \alpha_t^2 \mathbf{C}_{pp} \end{bmatrix}.$$

Let  $\mathbf{P}_x = \text{diag}(\mathbf{I}_n, \mathbf{0}_{d \times d})$  and  $\mathbf{P}_p = \text{diag}(\mathbf{0}_{n \times n}, \mathbf{I}_d)$  be coordinate projectors. Reservoir features help only if they are retained in the top- $n$  eigenspace of  $\mathbf{C}_t(\alpha_t)$ , quantified by

$$E_p = \text{tr} \left( \mathbf{V}_n^\top \mathbf{P}_p \mathbf{C}_t(\alpha_t) \mathbf{P}_p \mathbf{V}_n \right), \quad (8)$$

$$E_x = \text{tr} \left( \mathbf{V}_n^\top \mathbf{P}_x \mathbf{C}_t(\alpha_t) \mathbf{P}_x \mathbf{V}_n \right), \quad (9)$$

$$\text{IER}_t = \frac{E_p}{E_x + E_p}, \quad \text{SSO}_t = \frac{\|\mathbf{P}_p \mathbf{V}_n\|_F^2}{\|\mathbf{V}_n\|_F^2}. \quad (10)$$

IER is the retained-energy share from reservoir coordinates, whereas SSO is the retained subspace-overlap fraction on reservoir coordinates (scale-insensitive). Since  $\mathbf{V}_n^\top \mathbf{V}_n = \mathbf{I}_n$ , we have  $\|\mathbf{V}_n\|_F^2 = n$  and  $\text{SSO}_t \in [0, 1]$ . We also track the *retained passthrough ratio*  $\rho_{x,t} = E_x / \text{tr}(\mathbf{C}_{xx})$ , i.e., passthrough variance retained after top- $n$  selection.

**Crowd-out-guarded controller.** We pose injection control as  $\max_{\alpha} \text{IER}(\alpha)$  subject to  $\rho_x(\alpha) \geq \rho_x^*$ , and implement a tracking rule:  $\alpha_t$  is driven up when  $\text{IER}_t < \text{IER}^*$  and penalized when  $\rho_{x,t} < \rho_x^*$ :

$$\delta_t = \kappa(\text{IER}^* - \text{IER}_t) - \kappa_g[\rho_x^* - \rho_{x,t}]_+ / \rho_x^*, \quad (11)$$

$$\alpha_{t+1} = \text{clip}(\alpha_t e^{\delta_t}, \alpha_{\min}, \alpha_{\max}), \quad (12)$$

where  $[\cdot]_+ = \max(\cdot, 0)$ ,  $\kappa > 0$  is the IER tracking gain,  $\kappa_g > 0$  is the guard gain, and  $[\alpha_{\min}, \alpha_{\max}]$  are clipping bounds. We set  $\rho_x^*$  conservatively (e.g., 0.95) to retain  $\geq 95\%$  passthrough variance; performance is insensitive to the exact value as long as operation avoids the crowd-out regime ( $\rho_x < 0.9$ ; Table II). Similarly,  $\text{IER}^*$  is set as a practical operating target for stable online operation under the stated protocol. The update uses already-computed covariance/eigenspace statistics.

**Proposition 3** (Reservoir-entry condition (block-diagonal case)). *Let  $\tilde{\mathbf{C}}_t$  be block-partitioned as  $\begin{bmatrix} \mathbf{C}_{xx} & \mathbf{C}_{xp} \\ \mathbf{C}_{px} & \mathbf{C}_{pp} \end{bmatrix}$  under  $\tilde{\mathbf{u}}_t = [\mathbf{x}_t; \mathbf{p}_t]$ , and assume  $\mathbf{C}_{xp} = \mathbf{0}$ . If*

$$\lambda_{\max}(\alpha_t^2 \mathbf{C}_{pp}) > \lambda_n(\mathbf{C}_{xx}), \quad (13)$$

where  $\lambda_n(\mathbf{C}_{xx})$  denotes the  $n$ -th largest eigenvalue of  $\mathbf{C}_{xx}$ , then at least one top- $n$  eigenvector has nonzero reservoir component, so  $\text{SSO}_t > 0$ .

*Sketch.* With  $\mathbf{C}_{xp} = \mathbf{0}$  in  $\tilde{\mathbf{C}}_t$ ,  $\mathbf{C}_t(\alpha_t) = \text{diag}(\mathbf{C}_{xx}, \alpha_t^2 \mathbf{C}_{pp})$ , so its spectrum is the union of the spectra of the two blocks.

The stated strict inequality implies at least one reservoir-block eigenvalue enters the top- $n$  set, so the retained eigenspace has nonzero reservoir overlap.  $\square$

*Observation (crowd-out in the block-diagonal case).* Under  $\mathbf{C}_{xp} = \mathbf{0}$  in  $\tilde{\mathbf{C}}_t$ , if  $\lambda_{\max}(\alpha_t^2 \mathbf{C}_{pp}) > \lambda_n(\mathbf{C}_{xx})$ , at least one reservoir-dominated direction enters the top- $n$  eigenspace and replaces a passthrough direction, implying a decrease in  $\rho_{x,t}$ . For  $\mathbf{C}_{xp} \neq \mathbf{0}$  in  $\tilde{\mathbf{C}}_t$ , coupling in  $\mathbf{C}_t(\alpha_t)$  perturbs this ordering. With a non-negligible eigengap around  $\lambda_n(\mathbf{C}_{xx})$  and moderate  $\|\mathbf{C}_{xp}\|$ , Davis–Kahan-type bounds imply continuous variation from the block-diagonal limit; crowd-out can still arise when reservoir-induced variance becomes competitive in the top- $n$  spectrum.

*Remark.* The block-diagonal limit makes the mechanism explicit: top- $n$  selection is a competition between passthrough and reservoir block spectra. In experiments, normalized cross-block coherence is approximately constant across injection strengths, so performance changes are driven mainly by relative block energies rather than large coupling shifts.

**Interpretation.** In the block-diagonal limit,  $\text{SSO} > 0$  (Proposition 3) is necessary for reservoir influence but not sufficient for improved separation: when reservoir eigenvalues displace passthrough eigenvalues from the top- $n$  basis,  $\rho_x$  drops and SI-SDR degrades (*crowd-out*; see Table II for quantification). The guarded controller (11) mitigates this by adapting  $\alpha_t$  to maintain  $\rho_{x,t}$  near  $\rho_x^*$  in practice.

### E. Online Whitening and Natural Gradient ICA

**Online whitening.** For  $\mathbf{u}_t = [\mathbf{x}_t; \alpha_t \mathbf{p}_t] \in \mathbb{R}^{n+d}$ , we update the mean and covariance with forgetting factor  $\lambda \in (0, 1)$ :

$$\boldsymbol{\mu}_t = \lambda \boldsymbol{\mu}_{t-1} + (1 - \lambda) \mathbf{u}_t, \quad (14)$$

$$\mathbf{C}_t = \lambda \mathbf{C}_{t-1} + (1 - \lambda) (\mathbf{u}_t - \boldsymbol{\mu}_t)(\mathbf{u}_t - \boldsymbol{\mu}_t)^\top. \quad (15)$$

Before eigendecomposition we apply diagonal loading  $\mathbf{C}_t \leftarrow \mathbf{C}_t + \varepsilon \mathbf{I}$  ( $\varepsilon = 10^{-6}$ ). Every  $\Delta_w$  steps, we compute the top- $n$  eigenspace  $\mathbf{V}_n$  and eigenvalues  $\mathbf{D}_n$ , form  $\mathbf{W}_{\text{wh}} = \mathbf{D}_n^{-1/2} \mathbf{V}_n^\top$ , and whiten  $\mathbf{z}_t = \mathbf{W}_{\text{wh}}(\mathbf{u}_t - \boldsymbol{\mu}_t) \in \mathbb{R}^n$ . At each refresh we evaluate IER/SSO and  $\rho_{x,t}$  using the current top- $n$  eigenspace and update  $\alpha_{t+1}$  via (11);  $\alpha_t$  is held fixed between refreshes. Retaining top- $n$  eigenvectors matches the source count and removes low-variance directions; RSI controls whether reservoir directions remain in this retained subspace.

**Natural gradient ICA.** On  $\mathbf{z}_t$ , we update the demixing matrix  $\mathbf{W}_t \in \mathbb{R}^{n \times n}$  via the natural gradient [10]:

$$\mathbf{W}_{t+1} = \mathbf{W}_t + \eta (\mathbf{I}_n - \phi(\mathbf{y}_t) \mathbf{y}_t^\top) \mathbf{W}_t, \quad \mathbf{y}_t = \mathbf{W}_t \mathbf{z}_t, \quad (16)$$

where  $\phi = \tanh$  and  $\eta > 0$ . Every  $\Delta_o$  steps we apply  $\mathbf{W} \leftarrow (\mathbf{W} \mathbf{W}^\top)^{-1/2} \mathbf{W}$  to prevent drift.

**Algorithm 1 (RSI-controlled RE-OICA).** Per sample: update  $\mathbf{r}_t, \mathbf{p}_t$ ; form  $\mathbf{u}_t = [\mathbf{x}_t; \alpha_t \mathbf{p}_t]$ ; on refresh recompute top- $n$  whitening, evaluate IER/SSO/ $\rho_{x,t}$ , and update  $\alpha_{t+1}$  via (11); whiten to  $\mathbf{z}_t$ ; apply (16).

TABLE I  
LAST 5 000 SAMPLES (10 SEEDS, MEAN $\pm$ SEM): SI-SDR<sub>sc</sub> (DB), MEAN  $|r|$ , COUNT (RE-OICA > VANILLA).

Regime	Method	SI-SDR <sub>sc</sub>	Corr	Count
Static	RE-OICA	$-5.9 \pm 1.0$	$0.44 \pm 0.04$	6/10
	Vanilla	$-6.8 \pm 1.0$	$0.41 \pm 0.04$	
Time-var.	RE-OICA	$-6.0 \pm 1.1$	$0.44 \pm 0.04$	7/10
	Vanilla	$-6.1 \pm 1.1$	$0.44 \pm 0.04$	
Nonlinear	RE-OICA	$-7.0 \pm 1.1$	$0.41 \pm 0.04$	7/10
	Vanilla	$-8.7 \pm 1.0$	$0.35 \pm 0.03$	

FastICA (batch): static 35.4/1.00, time-var. 23.1/1.00, nonlinear 2.4/0.78 (SI-SDR<sub>sc</sub>/Corr).

## III. EXPERIMENTS

**Sources and mixing.** We use  $n=3$  standardized sources: Lorenz ( $x$ -component), Mackey–Glass ( $\tau=17$ ), and a linear chirp (0.5–5 Hz over 10 s). Mixing follows (1)–(3): static ( $\mathbf{A}$  fixed), time-varying ( $\varepsilon=0.3$ ,  $f=0.5$  Hz), and nonlinear ( $g=\tanh(\gamma)$ ,  $\gamma=0.8$ , SNR=10 dB with additive white Gaussian noise (AWGN)). Mixing matrices are random with condition numbers  $\leq 5$ .

**Methods.** We compare RE-OICA-base (ESN reservoir:  $N=500$ , sparsity 5%,  $\rho=0.95$ ,  $\alpha_r=0.1$ ,  $c_{\text{in}}=0.1$  input scaling, fixed random  $\mathbf{W}_{\text{read}} \in \mathbb{R}^{d \times N}$  with  $d=20$ , baseline  $c_N=1/N$ ), RE-OICA-sqrt ( $c_N=1/\sqrt{N}$ ), RE-OICA-RSI (guarded (11) with  $\text{IER}^*=0.25$ ,  $\rho_x^*=0.95$ ,  $\kappa=0.3$ ,  $\kappa_g=3$ ,  $\alpha_t \in [0.1, 10]$ ), an unguarded RSI counterfactual ( $\text{IER}^*=0.25$ , no  $\rho_x$  guard), and baselines vanilla online ICA and FastICA. All online methods share the same backend: EMA whitening ( $\lambda=0.995$ ,  $\Delta_w=64$ ) and natural-gradient ICA ( $\eta=5 \times 10^{-3}$ ,  $\Delta_o=50$ ). Vanilla online ICA (ORICA-inspired) applies this backend directly to  $\mathbf{x}_t$  without reservoir expansion (same natural-gradient update as ORICA [12], but EMA plus periodic eigendecomposition whitening rather than ORICA’s RLS whitening). FastICA [4] is the offline reference (full batch,  $\log \cosh$  nonlinearity; cf. [2], [31]). Online runs use a 1000-sample whitening warm-up (ICA frozen) and 2000-sample learning-rate ramp; Fig. 1(a) reports 10-seed mean $\pm$ standard error of the mean (SEM) running unshifted SI-SDR.

**Metrics and alignment.** On the last 5,000 samples, we compute lag-aware correlations  $\rho_{ij} = \max_{|\tau| \leq 200} |\text{corr}(s_i, y_j^{(\tau)})|$  and use Hungarian matching on  $[\rho_{ij}]$  to obtain a permutation  $\pi$ ; matched outputs are evaluated at their maximizing lags on the overlap. We report SI-SDR<sub>sc</sub> [32], [33], mean  $|r|$ , and RSI diagnostics (IER/SSO and  $\rho_x$ ). Running curves show trailing 2,000-sample *unshifted* SI-SDR, whereas steady-state SI-SDR<sub>sc</sub> is lag-compensated. Results are 10-seed mean $\pm$ SEM; counts are descriptive.

**Results (Fig. 1, Table I).** (a) *Convergence.* Under time-varying mixing, Fig. 1(a) shows 10-seed mean $\pm$ SEM running unshifted SI-SDR; both methods stabilize after  $\sim 3,000$  samples.

(b) *Cross-regime comparison (Table I).* Under this protocol, RE-OICA outperforms vanilla in all three regimes, with the largest gain under nonlinear mixing (+1.7 dB; Table I). FastICA is an offline reference in this benchmark; online SI-SDR<sub>sc</sub> is negative on these chaotic/oscillatory stress-test sources, where even batch FastICA reaches only +2.4 dB

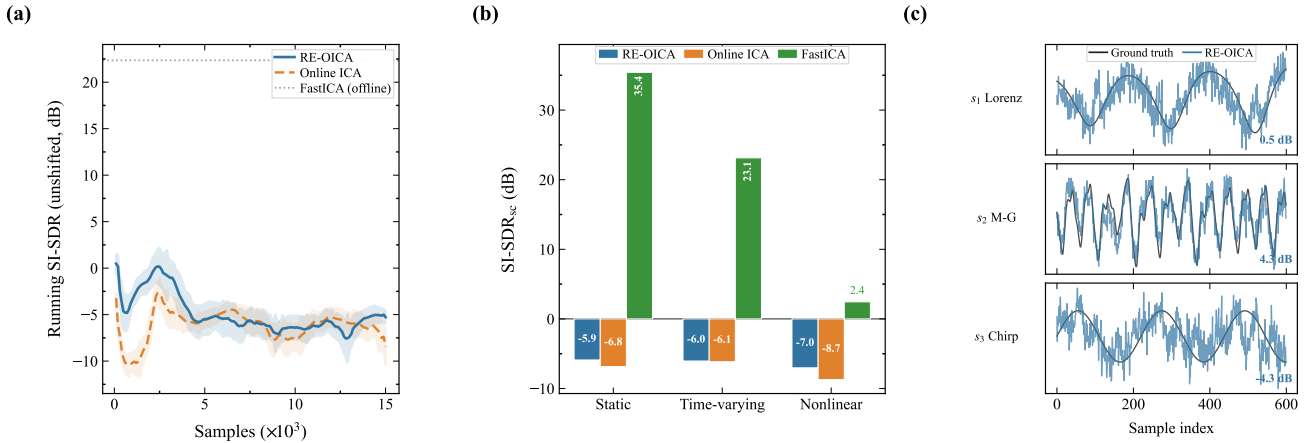


Fig. 1. RE-OICA validation ( $T=15,000$ ,  $n=3$ , 10 seeds). (a) Running unshifted SI-SDR (trailing 2000): RE-OICA, vanilla, FastICA. (b) Steady-state  $\text{SI-SDR}_{\text{sc}}$  across regimes (lag-compensated). (c) Nonlinear overlay (last 600): true vs. RE-OICA; corner labels show per-source unshifted SI-SDR.

under nonlinear mixing. Win counts are descriptive rather than inferential.

*Standard BSS validation.* On standard super-Gaussian sources (Laplace, square wave, sawtooth;  $T=30,000$ ; same mixing-matrix protocol with condition number  $\leq 5$  and same whitening/ICA hyperparameters), RE-OICA-base ( $1/N$  scaling) achieves  $+0.6 \pm 1.2$  dB vs.  $-2.9 \pm 2.3$  dB for vanilla ( $\Delta=+3.5$  dB, 7/10 seeds). Under mild nonlinearity ( $g=\tanh(0.5\cdot)$ ,  $\text{SNR}=20$  dB), RE-OICA-base achieves  $-1.5 \pm 1.0$  dB vs.  $-3.6 \pm 1.4$  dB ( $\Delta=+2.1$  dB, 9/10 seeds). Negative chaotic-source values are therefore consistent with task difficulty under this protocol.

(c) *Waveform quality.* Overlay (nonlinear, last 600 samples) shows RE-OICA tracks Lorenz and chirp dynamics qualitatively; Mackey–Glass remains the most difficult source (Fig. 1(c)).

*Computational cost.* Per-sample cost is dominated by reservoir encoding (sparse  $\mathbf{W}_{\text{res}}$  multiply,  $O(\text{nnz})$  with  $\text{nnz} = \text{nnz}(\mathbf{W}_{\text{res}})$ ); the  $O((d+n)^3/\Delta_w)$  amortized eigendecomposition and  $O(n^2)$  ICA update are modest for  $d+n=23$ ,  $n=3$  in our implementation setting.

**Ablation studies (Fig. 2, Table II).** All ablations follow the same protocol (10 seeds) and  $\text{SI-SDR}_{\text{sc}}$  evaluation.

(a) *N-sweep and RSI mechanism (Fig. 2(a), Table II).* Under baseline  $1/N$  scaling,  $\text{SI-SDR}_{\text{sc}}$  is nearly flat across  $N$  with very low IER and  $\rho_x \approx 1$ . Unconstrained  $1/\sqrt{N}$  scaling increases IER but degrades  $\text{SI-SDR}_{\text{sc}}$  via crowd-out, while the guarded RSI branch recovers near-baseline performance (Table II).

(b) *Architecture (Fig. 2(b)).* Recurrent ESN and memoryless random features (RF) perform similarly and are slightly above vanilla under time-varying mixing ( $\Delta=+0.1$ – $0.2$  dB), suggesting that, in this benchmark, high-dimensional nonlinear expansion is likely the primary contributor to the gain rather than fading memory.

(c) *Drift strength (Fig. 2(c)).* Across  $\varepsilon \in \{0.1, 0.3, 0.8\}$ , RE-OICA remains comparable to or slightly above vanilla ( $\Delta=+0.1$ – $0.8$  dB) with no monotonic dependence on  $\varepsilon$ .

Additional ablations on readout dimension, passthrough

TABLE II  
NONLINEAR (10 SEEDS):  $\text{SI-SDR}_{\text{sc}}$  (dB, MEAN  $\pm$  SEM),  $\text{IER}/\rho_x$   
STEADY-STATE, COUNT VS. RE-OICA-BASE.

Branch	$\text{SI-SDR}_{\text{sc}}$	IER	$\rho_x$	Count
RE-OICA-base ( $1/N$ )	$-7.0 \pm 1.1$	$<0.001$	1.00	(ref)
RE-OICA-sqrt ( $1/\sqrt{N}$ )	$-8.7 \pm 1.0$	0.016	0.94	2/10
RSI-unguarded (counterfactual, $\text{IER}^*=0.25$ )	$-9.2 \pm 1.0$	0.255	0.77	2/10
RE-OICA-RSI (guarded, $\rho_x^*=0.95$ )	$-7.1 \pm 1.1$	0.007	0.98	5/10

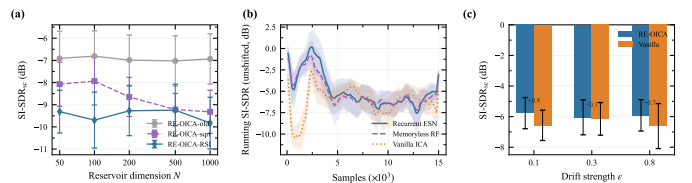


Fig. 2. Ablation studies (10 seeds, mean  $\pm$  SEM). (a)  $N$ -sweep under nonlinear mixing across three scaling branches. (b) Architecture: ESN vs. RF vs. vanilla (time-varying). (c) Drift sweep:  $\varepsilon \in \{0.1, 0.3, 0.8\}$ .

removal, and nonlinearity type showed qualitatively consistent trends (results not shown due to space constraints).

**Mechanism summary (Table II).** RSI diagnostics reveal a crowd-out tradeoff: increasing IER can reduce passthrough retention  $\rho_x$  and degrade  $\text{SI-SDR}_{\text{sc}}$ , while the guarded controller preserves  $\rho_x$  and recovers near-baseline performance. Cross-block coherence remains stable (0.38–0.45), suggesting increased reservoir-block energy  $\|\mathbf{C}_{pp}\|$  rather than coupling changes.

#### IV. CONCLUSION

Top- $n$  whitening makes reservoir expansion a rank-budget problem: features outside the retained eigenspace cannot help. RSI diagnostics (IER, SSO,  $\rho_x$ ) predict outcome; stronger injection can raise IER yet reduce  $\rho_x$  and  $\text{SI-SDR}$  (Table II). A low-overhead guarded controller maintains  $\rho_x \approx \rho_x^*$  and recovers mean performance to within 0.1 dB of baseline  $1/N$  scaling under our protocol. Future work should increase *useful* cross-block structure rather than merely  $\|\mathbf{C}_{pp}\|$ .

## REFERENCES

- [1] P. Comon, "Independent component analysis, a new concept?" *Signal Processing*, vol. 36, no. 3, pp. 287–314, 1994.
- [2] A. Hyvärinen, J. Karhunen, and E. Oja, *Independent Component Analysis*. Wiley, 2001.
- [3] A. J. Bell and T. J. Sejnowski, "An information-maximization approach to blind separation and blind deconvolution," *Neural Computation*, vol. 7, no. 6, pp. 1129–1159, 1995.
- [4] A. Hyvärinen, "Fast and robust fixed-point algorithms for independent component analysis," *IEEE Transactions on Neural Networks*, vol. 10, no. 3, pp. 626–634, 1999.
- [5] J.-F. Cardoso and A. Souloumiac, "Blind beamforming for non-Gaussian signals," *IEEE Proceedings F (Radar and Signal Processing)*, vol. 140, no. 6, pp. 362–370, 1993.
- [6] V. D. Calhoun, T. Adali, G. D. Pearlson, and J. J. Pekar, "A method for making group inferences from functional MRI data using independent component analysis," *Human Brain Mapping*, vol. 14, no. 3, pp. 140–151, 2001.
- [7] V. D. Calhoun and T. Adali, "Multisubject independent component analysis of fMRI: a decade of intrinsic networks, default mode, and neurodiagnostic discovery," *IEEE Reviews in Biomedical Engineering*, vol. 5, pp. 60–73, 2012.
- [8] A. Hyvärinen and E. Oja, "Independent component analysis: Algorithms and applications," *Neural Networks*, vol. 13, no. 4–5, pp. 411–430, 2000.
- [9] J.-F. Cardoso, "Blind signal separation: Statistical principles," *Proceedings of the IEEE*, vol. 86, no. 10, pp. 2009–2025, 1998.
- [10] S.-i. Amari, "Natural gradient works efficiently in learning," *Neural Computation*, vol. 10, no. 2, pp. 251–276, 1998.
- [11] S.-i. Amari, A. Cichocki, and H. H. Yang, "A new learning algorithm for blind signal separation," in *Advances in Neural Information Processing Systems*, vol. 8. MIT Press, 1996, pp. 757–763.
- [12] S.-H. Hsu, T. Mullen, T.-P. Jung, and G. Cauwenberghs, "Real-time adaptive EEG source separation using online recursive independent component analysis," *IEEE Transactions on Neural Systems and Rehabilitation Engineering*, vol. 24, no. 3, pp. 309–320, 2016.
- [13] C. J. Li and M. I. Jordan, "Stochastic approximation for online tensorial independent component analysis," 2021, arXiv preprint arXiv:2012.14415.
- [14] T. Kim, T. Eltoft, and T.-W. Lee, "Independent vector analysis: An extension of ICA to multivariate components," in *International Conference on Independent Component Analysis and Signal Separation*. Springer, 2006, pp. 165–172.
- [15] M. Anderson, G.-S. Fu, R. Phlypo, and T. Adali, "Independent vector analysis: Identification conditions and performance bounds," *IEEE Transactions on Signal Processing*, vol. 62, no. 17, pp. 4399–4410, 2014.
- [16] A. Taleb and C. Jutten, "Source separation in post-nonlinear mixtures," *IEEE Transactions on Signal Processing*, vol. 47, no. 10, pp. 2807–2820, 1999.
- [17] F. R. Bach and M. I. Jordan, "Kernel independent component analysis," *Journal of Machine Learning Research*, vol. 3, no. Jul, pp. 1–48, 2002.
- [18] A. Hyvärinen, I. Khemakhem, and H. Morioka, "Nonlinear independent component analysis for principled disentanglement in unsupervised deep learning," *Patterns*, vol. 4, no. 10, 2023.
- [19] A. Hyvärinen and H. Morioka, "Unsupervised feature extraction by time-contrastive learning and nonlinear ica," in *Advances in Neural Information Processing Systems*, vol. 29, 2016, pp. 3765–3773.
- [20] I. Khemakhem, D. Kingma, R. Monti, and A. Hyvärinen, "Variational autoencoders and nonlinear ica: A unifying framework," in *Proceedings of the Twenty Third International Conference on Artificial Intelligence and Statistics*, ser. Proceedings of Machine Learning Research, vol. 108, 2020, pp. 2207–2217.
- [21] H. Jaeger, "The "echo state" approach to analysing and training recurrent neural networks," German National Research Center for Information Technology (GMD), Tech. Rep. 148, 2001.
- [22] H. Jaeger and H. Haas, "Harnessing nonlinearity: Predicting chaotic systems and saving energy in wireless communication," *Science*, vol. 304, no. 5667, pp. 78–80, 2004.
- [23] M. Lukoševičius, "A practical guide to applying echo state networks," in *Neural Networks: Tricks of the Trade*, 2nd ed., G. Montavon, G. B. Orr, and K.-R. Müller, Eds. Springer, 2012, pp. 659–686.
- [24] J. Dong, R. Ohana, M. Rafaël, C. Raffel, F. Krzakala, S. Gigan, and L. Daudet, "Reservoir computing meets recurrent kernels and structured transforms," in *Advances in Neural Information Processing Systems*, vol. 33, 2020, pp. 16 785–16 796.
- [25] P. Singh and B. Raman, "Echo state networks as state-space models: A systems perspective," 2025, arXiv preprint arXiv:2509.04422.
- [26] J. Choi and P. Kim, "Signal-noise separation using unsupervised reservoir computing," 2024, arXiv preprint arXiv:2404.04870.
- [27] I. B. Yildiz, H. Jaeger, and S. J. Kiebel, "Re-visiting the echo state property," *Neural Networks*, vol. 35, pp. 1–9, 2012.
- [28] L. Grigoryeva and J.-P. Ortega, "Echo state networks are universal," *Neural Networks*, vol. 108, pp. 495–508, 2018.
- [29] A. Rahimi and B. Recht, "Random features for large-scale kernel machines," in *Advances in Neural Information Processing Systems*, vol. 20, 2007, pp. 1177–1184.
- [30] R. Vershynin, *High-Dimensional Probability: An Introduction with Applications in Data Science*. Cambridge University Press, 2018, vol. 47.
- [31] J. Miettinen, K. Nordhausen, H. Oja, S. Taskinen, and J. Virta, "The squared symmetric fastica estimator," *Signal Processing*, vol. 131, pp. 402–411, 2017.
- [32] J. Le Roux, S. Wisdom, H. Erdogan, and J. R. Hershey, "SDR – half-baked or well done?" in *Proceedings of the IEEE International Conference on Acoustics, Speech, and Signal Processing (ICASSP)*, 2019, pp. 626–630.
- [33] E. Vincent, R. Gribonval, and C. Févotte, "Performance measurement in blind audio source separation," *IEEE Transactions on Audio, Speech, and Language Processing*, vol. 14, no. 4, pp. 1462–1469, 2006.